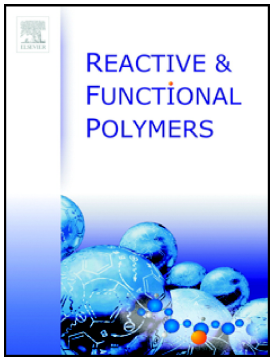

Glutathione and endosomal pH-responsive hybrid vesicles fabricated by zwitterionic polymer block poly(l-aspartic acid) as a smart anticancer delivery platform

Renjith P. Johnson, Saji Uthaman, Rimesh Augustine, Yu Zhang, Hwa Jin, Chang In Choi, In-Kyu Park, Il Kim

PII: S1381-5148(17)30138-4
DOI: doi: 10.1016/j.reactfunctpolym.2017.07.010
Reference: REACT 3884

To appear in: *Reactive and Functional Polymers*

Received date: 22 May 2017
Revised date: 10 July 2017
Accepted date: 29 July 2017

Please cite this article as: Renjith P. Johnson, Saji Uthaman, Rimesh Augustine, Yu Zhang, Hwa Jin, Chang In Choi, In-Kyu Park, Il Kim , Glutathione and endosomal pH-responsive hybrid vesicles fabricated by zwitterionic polymer block poly(l-aspartic acid) as a smart anticancer delivery platform, *Reactive and Functional Polymers* (2017), doi: 10.1016/j.reactfunctpolym.2017.07.010

Glutathione and endosomal pH-responsive hybrid vesicles fabricated by zwitterionic polymer block poly(*L*-aspartic acid) as a smart anticancer delivery platform

Renjith P. Johnson[a,1], Saji Uthaman[b], Rimesh Augustine[a], Yu Zhang[a], Hwa Jin[a], Chang In Choi[c], In-Kyu Park[b], Il Kim[a,*]

[a] *BK21 PLUS Centre for Advanced Chemical Technology, Department of Polymer Science and Engineering, Pusan National University, Busandaehak-ro 63, Geumjeong-gu, Busan, 46241, Republic of Korea*

[b] *Department of Biomedical Science and BK 21 PLUS Center for Creative Biomedical Scientists, Chonnam National University Medical School, 160 Baekseo-ro, Gwanju, 501-746, Republic of Korea.*

[c] *Department of Surgery, Medical Research Institute, Pusan National University Hospital, Busan 602-739, South Korea*

[1] Present address: Yenepoya Research Centre, Yenepoya University, Mangalore, India

* Corresponding author. Tel: +82-51-510-2466. E-mail: ilkim@pusan.ac.kr

Abstract

Zwitterionic hybrid block copolymer based nanocarriers are ideal candidates for drug delivery applications due the higher resistance to nonspecific protein adsorption in complex media compared to nonionic polymers. Especially, zwitterionic poly(2-methacryloyloxyethyl phosphorylcholine) p(MPC) based nanocarriers can maintain its stability during circulation in complex media, such as serum. Thus, a series of bioreducible and pH-responsive zwitterionic/amphiphilic block copolymers, poly(2-methacryloyloxyethyl phosphorylcholine)$_{50}$-*block*-poly(L-aspartic acid)$_n$ (p(MPC)$_{50}$–*b*–p(AA)$_n$) (n = 10, 25, 50, 75), bearing a degradable disulfide linker have been synthesized and exploited as dual-stimuli-responsive drug delivery vehicle of the chemotherapeutic drug, doxorubicin (Dox). Dox was successfully loaded into uniform vesicles (~100 nm) fabricated from p(MPC)$_{50}$–*b*–p(AA)$_n$ and the release performance was investigated under different pH conditions and with a range of concentrations of the reducing agent, 1,4-dithiothreitol (DTT). At physiological conditions, increasing concentrations of DTT resulted in faster Dox release from vesicles. Dox release at elevated DTT concentrations was more effective at pH 5.5 than at pH 7.5. Blank vesicles were non-toxic over a wide concentration range when tested in normal cell lines (0.01–100 μg/mL). Vesicles efficiently encapsulated Dox and the dual stimuli-responsive disassembly results demonstrated controlled and sustained release of Dox tin 4T1 cancer cells to confer dose-dependent cytotoxicity. Thus, the bioreducible and pH sensitive vesicles appear to be a promising theranostic platform for drug delivery applications.

Keywords: Biodegradation, Block copolymer, Drug delivery, Polypeptide, Responsive polymer

1. Introduction

Chemotherapeutic drug delivery vehicles such as polymer drug conjugates [1], liposomes [2], polymeric micelles [3–5], and polymersomes [6, 7] (vesicles of synthetic amphiphilic block copolymers) have been widely investigated in recent decades for tumor-targeted treatments. Generally, these nano-vehicles enhance the solubility and bioavailability of drugs, allowing the drug to act directly at the target site of interest. By avoiding rapid clearance by the reticuloendothelial system (RES), these carriers can have a long circulation time. This contributes to accumulation at the tumor site through the enhanced permeability and retention (EPR) effect that occurs in response to abnormalities of tumor blood and the lymphatic vasculature [8, 9]. However, several drawbacks to applications of these carriers still persist, including systemic toxicity, reduced intracellular uptake, and poor endosomal escape after the cellular entry [10–12].

"Smart" polymeric nano-vehicles can respond to physiological conditions *in vivo*, such as pH [13, 14], temperature [15], certain enzymes [16], redox substances [17], and even multiple stimuli. This attracted great attention in the drug delivery domain. Undoubtedly, pH is one of the most frequently exploited physiological stimuli owing to the significant pH difference between blood and extracellular matrices and that of intracellular compartments [18]. To date, several pH-responsive delivery vehicles, including micelles or vesicles, have been developed to target tumor tissue or cellular compartments [3, 6]. "Titratable" groups such as imidazoles, tertiary amines, and carboxylic acid-containing amphiphilic block copolymer assemblies can exhibit a "proton-sponge" effect in acidic environments and these have been designed for intracellular-targeted

drug release [19–21]. Recently, we developed poly(L-histidine)-based hybrid materials for pH or pH/temperature dual responsive nano-vehicles for cancer therapy [4, 5, 22, 23].

In recent decades, parallel progress has been made by several research groups in the design of bioreducible nano-carriers for triggered intracellular release of anticancer drugs [6, 24]. The basic principle behind the use of bioreducible carriers is the cleavage of the disulfide (SS) bond of the molecular structures, either when located in the main chain, at the side chain, or as a cross-linker, upon exposure to reductive intracellular environments. The abundance of the SS-reducing biological thiol, glutathione tripeptide (L-γ-glutamyl-L-cysteinyl-glycine; GSH) is much higher in the cytosol than in the blood and other extracellular fluids (2−10 mM in cytosol vs. 2−20 μM in extracellular fluids) [25]. Thus, the SS bonds are sufficiently stable in the circulating blood and in the extracellular environment, but can undergo rapid cleavage through the thiol–disulfide exchange reaction, at a time scale of minutes to hours, under more reductive intracellular environment [26]. Additionally, tumor tissues are highly reducing and hypoxic when compared with normal tissues [27] and contain at least 4-fold higher concentrations of GSH.

The characteristic acidic and reductive tumor environment demands the design and synthesis of multi-stimuli responsive vehicles for attaining an improved therapeutic effect. Even though liposomes and micelles have been investigated as major platforms for the delivery of anticancer drugs and imaging agents, it is recognized that pure liposomes suffer from very rapid blood clearance *in vivo* by the RES, unless a surface modification approach is applied. Recently, polymer vesicles have attracted increasing interest owing to their cell-and virus-mimicking dimensions, function, and their ability to overcome the chemical and physical limits of liposomes and micelles [28, 29]. To date, the syntheses of several amphiphilic block copolymers and the fabrication of their vesicles have been reported. The first-generation polymer vesicles [30–32]

were derived from block copolymers that were not completely biodegradable, which was a major drawback limiting their biomedical utility. Over the last decade, pure polypeptidic [33] and polypeptide-hybrid vesicles or hydrogels have emerged, and these have been investigated for delivery of the anticancer drug doxorubicin hydrochloride (Dox) [34–39].

In the past decades, polyethylene glycol (PEG) was the most common choice as a hydrophilic biocompatible segment in designing various polymeric drug carriers. However, PEG with lower molecular weight (i.e., less than 3000) was cytotoxic in the body [40]. Recently, poly(2-hydroxyethyl methacrylate) [41] and poly[2-(methacryloyloxy)ethyl phosphorylcholine] [p(MPC)] were emerged as alternatives for PEG. Interestingly, MPC is a zwitterionic, hemocompatible and highly hydrophilic monomer, which mimicks the phospholipid headgroups located on the surface of cell membranes, remarkably resistant to protein adsorption as well as bacterial/cellular adhesion [42]. Additionally, p(MPC) has been widely implemented in surface modification as biomaterials that exhibit exceptional hydrophilicity, biocompatibility, and antifouling properties [43]. Thus, in order to overcome the limitation of liposomes and micelles by fabricating pH/reduction dual-responsive vesicles from block copolymer composed of p(MPC) and relatively hydrophobic and pH-responsive poly(L-aspartic acid) [p(AA)] is designed.

Herein, we have synthesized a block copolymer poly(2-(methacryloyloxy)ethyl phosphorylcholine)$_{50}$–*b*–poly(L-aspartic acid)$_n$ (p(MPC)$_{50}$-*b*-p(AA)$_n$) (n= 10, 25, 50, 75) bearing a redox responsive disulfide (–SS–) linker for the triggered delivery of Dox. The synthesis employed reversible addition fragmentation chain transfer (RAFT) polymerization, ring-opening polymerization (ROP) of *β*-benzyl-L-aspartate *N*-carboxyanhydride (BLA–NCA) and click-cycloaddition reactions. pH and reduction dual-responsive vesicles for encapsulation of Dox were fabricated. The successful redox and pH-responsive *in vitro* release of Dox was

investigated and the cytotoxicity of the vesicles assessed in mouse embryonic fibroblast (NIH 3T3) and mouse mammary tumor (4T1) cell lines; the anticancer effect of the released Dox was confirmed in 4T1 cell lines.

2. Experimental

2.1. Materials

4-(Dimethylamino)pyridine (DMAP, 99%), N,N′-dicyclohexylcarbodiimide (DCC, 99.0%), 2,2′-azobis(2-methylpropionitrile (AIBN 98%), 3-bromo-1-propanol, 2-bromo-2-phenylacetic acid, sodium thiomethoxide ($NaSCH_3$-21% in water), carbon disulfide CS_2, 99.9%), 2-methacryloyloxyethyl phosphorylcholine (MPC, 97%), 1,1′-carbonyldiimidazole, propargyl alcohol (99%), cystamine dihydrochloride (96%), β-benzyl-L-aspartate (BLA) and anhydrous N,N-dimethylformamide (DMF) were purchased from Sigma-Aldrich. Dox was purchased from Lancrix Chemicals (Shanghai, China). Hexylamine (99.9%), trifluoroacetic acid (99%), HBr (33 wt% in acetic acid), sodium azide, and triphosgene (>98%) were purchased from TCI (Tokyo, Japan). Tetrahydrofuran (THF), methanol, chloroform, and dichloromethane (DCM) were dried over calcium hydride and distilled under reduced pressure. All other reagent-grade chemicals were purchased from Daejung Chemicals (Siheung, Korea) and used without further purification. Deionized (DI) water (purified to a resistance of 18 MΩ (Milli−Q Reagent Water System, Millipore Corp., Billerica, MA, USA) was used in all solution preparations, polymer isolations, and necessary reactions.

2.2. General methods

All column chromatography purifications were performed using a Combi-Flash companion purification system (Teledyne ISCO) with silica gel of 300-400 mesh. ^{1}H-NMR (400 MHz) and

^{13}C-NMR (100 MHz) spectra were recorded on a Varian INOVA 400 NMR spectrometer. Chemical shifts were reported in parts per million (ppm) relative to the residual solvent peaks as internal standard. Peak multiplicities in ^{1}H-NMR spectra are abbreviated as s (singlet), d (doublet), t (triplet), m (multiplet), and br (broad). Fourier-transform infrared (FT–IR) spectra were recorded using a Shimadzu IR prestige 21 spectrometer on KBr discs over the range of 3500–500 cm^{-1} at room temperature. UV−vis experiments conducted on a shimadzu UV-1650 PC. The molecular weight (MW) and polydispersity index (*Đ*) of the polymers were measured using a Waters GPC system, which was equipped with a Waters 1515 HPLC solvent pump, a Waters 2414 refractive index detector, and three Waters Styragel High-Resolution columns (HR4, HR2, HR1, effective molecular weight range 5000–500,000, 500–20,000, and 100–5000 g mol^{-1}, respectively) at 40 °C with HPLC-grade DMF containing 0.1 N LiBr as eluent at a flow rate of 1.0 mL/min. Monodispersed polystyrenes were used to generate the calibration curve. DLS measurements were performed with a high-performance Zetasizer Nano ZS90 (Malvern Instruments, Ltd., U.K.). Block copolymer solutions (2 mg·mL^{-1}) were filtered through a 0.5 μM filter prior to use. Transmission electron microscopy (TEM) was performed using a JEOL–1299EX TEM at an accelerating voltage of 80 keV.

2.3. Synthesis and polymerization. The general synthetic and polymerization procedures are presented in **Scheme 1**.

2.3.1. Synthesis of *S*-azidopropanoxycarbonylphenylmethyl trithiocarbonate (CTA–N_3)

For the RAFT polymerization of MPC, an azide-terminated chain transfer agent was synthesized by following the report of Ladmiral and coworkers [42,44]. The spectroscopic characterizations of the CTA–N_3 are provided in Fig. S1 of the Supplementary material (SM).

2.3.2. Synthesis of propargyl ester of carbonyl imidazole (PPA–CIM).

PPA–CIM was synthesized as described previously [45]. 1,1'-Carbonyldiimidazole (7.3 g, 45 mmol) and 50 mL DCM were added into a dry round-bottom flask. Then, propargyl alcohol (1.45 mL, 25 mmol) was added dropwise. The obtained clear solution was stirred at room temperature for 1 h, and washed with water (3×70 mL). The product was dried over magnesium sulfate, and evaporated to obtain PPA-CIM as an off-white solid. Yield: 80%. ^{1}H-NMR (400 MHz, $CDCl_3$, 298 K): δ (ppm) 8.19 (s, 1H, NCHN), 7.45 (s, 1H, NCHCHN), 7.10 (s, 1H, NCHCHN), 5.0 (s, 2H, OCH_2C), and 2.63 (s, 1H, CCH).

2.3.3. Synthesis of ((Propargyl carbamate)ethyl) Dithioethylamine (PPA–CAM).

Cystamine dihydrochloride was neutralized by 4 M NaOH and extracted with DCM to yield cystamine. PPA–CIM (1.44 g, 9.58 mmol) and cystamine (2.28 g, 15 mmol) were dissolved in 30 mL DCM and subsequently stirred at room temperature for 24 h. After evaporation of DCM, 25 mL of 1.0 M NaH_2PO_4 (pH 4.0) was added. This aqueous solution was extracted with diethyl ether (20 mL, 5 times) to remove the di-alkyne compound bis[(propargyl carbamate)ethyl] disulfide. The aqueous phase was basified with 1.0 M NaOH to pH 9.0, extracted with ethyl acetate (15 mL, 5 times), and dried over anhydrous magnesium sulfate. Rotary evaporation resulted in PPA–CAM as a pale yellow viscous liquid [43,45]. Yield: 42%. ^{1}H-NMR (400 MHz, $CDCl_3$, 298 K): δ (ppm) 2.45 (s, 1H, CH≡C), 2.75 (m, 4H, S–CH_2–C), 2.98 (m, 2H, NH_2–CH_2–C), 3.50 (m, 2H, NH–CH_2–C), 4.37 (b, 2H, NH_2–C), 4.64 (s, 2H, O-CH_2-C≡C), 5.58 (s, 1H, NH–C=O). The spectroscopic characterizations of the PPA–CAM are provided in Fig. S2 of SM.

2.3.4. RAFT Polymerization of MPC from CTA–N_3.

To a 10-mL Schlenk tube equipped with a magnetic stir bar, the following were added; MPC (1.48 g, 5 mmol), CTA–N_3 (34 mg, 0.1 mmol), AIBN (8 mg, 0.05 mmol), and methanol (5 mL). The [monomer]:[CTA]:[AIBN] ratio was 50:0.1:0.05. The solution was then degassed via three

freeze–vacuum–thaw cycles and placed in a 60 °C oil bath for 12 h. p(MPC)–N_3 was obtained by precipitating in excess acetone. See Fig. S3 of SM for FT-IR spectra.

2.3.5. Synthesis of BLA–NCA.

The synthesis of BLA–NCA was carried out using triphosgene. A suspension of BLA (4 g, 18 mmol) in 25 mL of THF was heated to 60 °C under nitrogen atmosphere. A solution of triphosgene (1.78 g, 6 mmol) dissolved in 25 mL of THF was added dropwise to the stirred reaction mixture. When the reaction mixture started to become transparent, a stream of dry nitrogen was bubbled through the solution to remove HCl. After the reaction was complete, the mixture was precipitated in anhydrous hexane. Further purification of the obtained Bn-ASP-NCA was accomplished by recrystallization from anhydrous THF/hexane followed by drying under vacuum at 40 °C. Yield: 87%. IR (KBr, cm^{-1}): 3312 (amide NH), 3000 (aromatic), 1870–1788 (cyclic anhydride, asym&sym. C=O str.mode), 1728 (ester C=O str.), 1640 (C=O amide I band), 1517 (amide II band) ^{1}H-NMR (400 MHz, DMF-d_6, 298 K): δ (ppm) 8.95 (CH–NH–C=O), 7.36–7.37 (Ph), 5.13 (CH_2–Ph), 4.69 (NH–CH), 2.8–3.0 (O=C–CH_2–CH) (see Fig. S4 of SM).

2.3.6. Synthesis of Alkyne-terminated p$(BLA)_n$ (n= 10, 25, 50, 75).

PPA–CAM (0.012 g, 0.05 mmol) and a prescribed amount of BLA–NCA were dissolved in absolute DMF (4 mL each) in two separate Schlenk flasks and subsequently combined using a transfer needle under nitrogen. The reaction mixture was stirred for 3 days at room temperature under nitrogen. After polymerization was complete, the solvent was concentrated, and precipitated in diethyl ether. The alkyne terminated p(BLA) (alkyne–p$(BLA)_n$) (n= 10, 25, 50, 75) was obtained after vacuum drying. The NMR spectrum of alkyne–p$(BLA)_{50}$) and GPC traces of alkyne–p$(BLA)_n$ (n = 10, 25, 50, 75) are provided in Fig. S5 of SM.

2.3.7. Synthesis of $p(MPC)_{50}$-b-$p(AA)_n$ (n = 10, 25, 50, 75).

The click cycloaddition reaction between $p(MPC)–N_3$ and alkyne–$p(BLA)_n$ was performed as follows. For example, $p(MPC)_{50}–N_3$ (0.35 g, 0.025 mmol) and alkyne–$p(BLA)_{50}$ (0.24 g, 0.025 mmol) were dissolved in a 25 mL Schlenk flask containing dry DMF (15 mL) connected with a nitrogen inlet and covered with a rubber septum. The mixture was stirred for 30 min and *N,N,N′,N″,N″*-pentamethyldiethylenetriamine (10 µL, 0.08 mmol) was added through a sterile syringe under nitrogen environment. The mixture was degassed over three freeze-thaw cycles and added to another Schlenk containing CuBr (0.011 g, 0.08 mmol) via a nitrogen-purged syringe. The Schlenk flask was placed in an oil bath maintained at 40 °C for 3 days under static nitrogen pressure. After the completion of the reaction, the solution was passed through a short silica column to remove copper catalyst, $p(MPC)_{50}$–*b*–$p(BLA)_{50}$ was precipitated by pouring into excess diethyl ether (see ^{1}H NMR spectrum in Fig. S6(A) of SM).

For the deprotection of the protective side groups, a round-bottomed flask was charged with a solution of $p(MPC)_{50}$–*b*–$p(BLA)_{50}$ in trifluoroacetic acid (250 mg, 5 mL). Then, a four-fold molar excess of a 33 wt% solution of HBr in acetic acid was added, the reaction mixture was stirred overnight at room temperature, and then precipitated in diethyl ether to obtain the deprotected block copolymer $p(MPC)_{50}$–*b*–$p(AA)_{50}$. The trithio moiety was subsequently removed by aminolysis, in presence of hexylamine (2 eq.) and few drops of $Na_2S_2O_4$ in DMF, and the block polymer was dialyzed against DI water for 24 h. The lyophilized $p(MPC)_{50}$–*b*–$p(AA)_{50}$ (see ^{1}H NMR spectrum in Fig. S6(B) of SM) stored at −20 °C. Other copolymers also were synthesized, purified and stored by similar procedure.

2.4. Fabrication of $p(MPC)_{50}$–b–$p(AA)_n$ vesicles.

The vesicles of p(MPC)$_{50}$–*b*–p(AA)$_n$ were prepared by combining a self-assembly derived nanoprecipitation with membrane dialysis against double distilled water. For example, p(MPC)$_{50}$–*b*–p(AA)$_{50}$ (1 mg) was dissolved in ethanol (0.5 mL), followed by the dropwise addition of phosphate buffer (PBS) (0.5 mL, pH 7.4, 50 mM) under stirring. The mixture was then heated to 50 °C for 2 h under static conditions, and allowed to cool slowly. The turbid mixture was then dialyzed against DI for 12 h using a dialysis membrane (Spectrapor, MWCO = 2000). The outer phase was replaced at 3-h intervals with fresh water, and finally the vesicles were lyophilized. TEM observation was performed directly after the deposition of the vesicle dispersion onto a Formvar carbon-coated copper grid after complete drying.

2.5. Reduction and pH-triggered destabilization of p(MPC)$_{50}$–b–p(AA)$_n$ vesicles.

The size change of the vesicles in response to the addition of 1,4-dithiothreitol (DTT) and pH change was determined by DLS measurements. The solution was mildly stirred at 37 °C and degassed in advance by purging nitrogen for 10 min, and then at different time intervals, the size of the vesicles was measured using a DLS spectrometer. Briefly, a 2 mL solution of p(MPC)$_{50}$–*b*–p(AA)$_{75}$ vesicles (1 mg/mL) in PBS was adjusted to the required pH, then to monitor the pH and reduction-responsive disassembly, 10 mmoL of DTT was added and the pH corrected before measurement.

2.6. Preparation of Dox-loaded p(MPC)$_{50}$–b–p(AA)$_n$ vesicles and in vitro Dox release.

For the fabrication of Dox–loaded p(MPC)$_{50}$–*b*–p(AA)$_{75}$ vesicles, Dox (2 mg) was dissolved in 0.5 mL of ethanol. The ethanolic solution of p(MPC)$_{50}$–*b*–p(AA)$_{75}$ (1 mg in 0.5 mL) and the Dox solution was then mixed and stirred for 2 h in the dark. PBS (0.5 mL, pH 10.5, 50 mM) was added under stirring and the mixture warmed to 50 °C for 2 h under static conditions. The solution was dialyzed using a membrane (Spectrapor, MWCO=2000) for 12 h to remove free

drug and then lyophilized in the dark. For quantification of the amount of drug encapsulated, aliquots of the drug-loaded vesicles were broken up by adding 1 mL of DMSO. The obtained solution was analyzed using UV–Vis spectroscopy. The characteristic absorbance of Dox (485 nm) was recorded and compared with a standard curve generated from a range of Dox concentrations in DMSO. The percentages of DLC and DLE were calculated according to the following equations.

$$\text{DLC (\%)} = \frac{\text{weight of Dox in the vesicles}}{\text{weight of Dox loaded vesicles}} \times 100$$

$$\text{DLE (\%)} = \frac{\text{weight of Dox in the vesicles}}{\text{weight of Dox for drug-loaded vesicle preparation}} \times 100$$

For reduction and pH-triggered *in vitro* Dox release studies, Dox–loaded vesicles were diluted to 1 mg/mL and then the solution was transferred into a dialysis membrane tubing (MWCO =10000). It was immersed into small beakers containing 20 mL of PBS buffer with fixed pH value and DTT concentrations to acquire the sink conditions and the solutions were incubated at 37° C in the dark in a shaking bath. At predetermined time intervals, the buffer solution was replaced (1 mL each) with fresh solution and the amount of the released drug was measured by UV–vis spectroscopy measurements. The drug concentration was determined according to the standard curves for the drug solution at different pH values.

2.7. Cell Viability Assay

In vitro cytotoxicity of blank and Dox-loaded $p(MPC)_{50}$–*b*–$p(AA)_n$ vesicles was assessed using NIH 3T3 and 4T1 cell lines. The cells were seeded in 96-well plates at a density of $1x10^4$ and incubated overnight at 37 °C before treatment. The media were then removed and $p(MPC)_{50}$–*b*–$p(AA)_n$ vesicle samples at a range of concentrations in OPTI-MEM® were added to the cells, which were then incubated at 37 °C for 6 h. The optimal media was then aspirated

and replaced with 100 µL of fresh media and incubated for 24 h at 37 °C. Cell viability profiles were assessed using the MTS assay. Briefly, 20 µL of MTS reagent was added to each well and incubated for 4 h; cell viability was determined by measuring the absorbance at 490 nm using a 550 BioRad plate-reader. The cell viability in each well was calculated from the measured values and presented as relative percentages using non- treated cells as a positive control. Results were presented as the mean and standard deviation, obtained from five different samples.

2.8. Confocal Laser Scanning Microscopy (CLSM) and Flow Cytometer Analysis

To perform CLSM, 4 T1 cells were seeded in a Lab-Tek® chamber slide at a density of 1×10^5 cells/well and incubated overnight prior to sample addition. The pH of the culture medium was regulated with 0.1 M HCl or 0.1 M NaOH to give the required pH. After overnight incubation, Dox loaded $p(MPC)_{50}$–*b*–$p(AA)_{75}$ vesicles were added to the 4T1 cells and incubated in the dark for 4 h at 37 °C. The media was then aspirated and cells were washed with PBS three times, followed by 4% paraformaldehyde treatment to fix the cells. Fluorescence was then visualized using confocal laser scanning microscope.

The flow cytometer analysis Dox loaded $p(MPC)_{50}$–*b*–$p(AA)_{75}$ vesicles were treated with 4T1 cells, seeded at a density of 1×10^6 cells/well were incubated overnight. The pH of the culture medium was regulated with 0.1 M HCl, or 0.1 M NaOH to a required pH prior to the treatment. After incubation, the medium was then aspirated and the cells were washed three times with PBS. After PBS wash, cells were collected and analyzed with flow cytometer. An excitation wavelength at 488 nm and emission wavelength at 522 nm were used to observe the Dox fluorescence intensity.

3. Results and Discussion

3.1. Synthesis of azide-terminated p(MPC) via RAFT polymerization

RAFT polymerization is well established as the most promising radical polymerization technique, owing to its ease of experimental setup and its applicability to a wide range of monomers. Trithiocarbonate CTAs offer flexibility for the design of functional copolymer architectures directly or after an appropriate end-group modification. The overall synthetic procedure of p(MPC)–*b*–p(AA)$_n$ (n = 10, 25, 50, 75) is shown in Scheme 1. We utilized CTA–N_3 bearing an azide group for the polymerization of MPC. The ^{1}H, ^{13}C-NMR and FT-IR spectra of the CTA–N_3 are provided in Fig. S1 of SM. The RAFT polymerization of MPC was conducted in methanol with [MPC]:[CTA]:[AIBN] feed ratios of 50:1:0.3. Polymerization was carried out over 12 h and the azide-terminated p(MPC) purified and isolated by precipitating in acetone. The number average MW (M_n) of the polymer was estimated using ^{1}H-NMR end-group analysis by integrating the signals corresponding to MPC (3.1 ppm) and to aromatic signals from the CTA portion (7.2 ppm). The calculated M_n was 14,000, which corresponds to about 48 repeating units of MPC and is close to the numbers obtained from theoretical calculations. The p(MPC)–N_3 was further characterized by FT-IR spectroscopy which revealing a characteristic band at 2100 cm^{-1} confirming the existence of azide groups in the polymer chain end (Fig. S3 of SM).

3.2. Synthesis of alkyne–p(BLA)$_n$

The synthesis of alkyne–p(BLA) was carried out using PPA–CAM as the initiator. The initiator structure was confirmed by ^{1}H, ^{13}C-NMR, and FT-IR spectral analyses (Fig. S2 of SM). Subsequently, the ring-opening polymerization of BLA–NCA was performed in anhydrous DMF and completed in a controlled manner in 1 to 3 days depending on the degree of polymerization to be obtained. The full conversion of the NCAs into p(BLA) was monitored and confirmed by the disappearance of the NCA-associated carbonyl peaks at 1795 and 1730 cm^{-1} in the FT-IR

spectra. The alkyne–p(BLA)$_n$ (n = 10, 25, 50, 75) polymers were precipitated in ethyl ether twice, and vacuum-dried. All polymers were characterized by ^{1}H-NMR spectra and the M_n values were calculated by comparing the peak integral ratios of the methylene group (4.9 ppm) and the aromatic signal (7.4 ppm) from p(BLA) units. Based on GPC characterization, the $Đ$ values of the block copolymers were found to be in the range of 1.2−1.3 (see Table S1). The ^{1}H-NMR spectra and the GPC elution curves of alkyne–p(BLA)$_n$ are provided in Fig. S5 of SM.

3.3. Synthesis of p(MPC)$_{50}$−b−p(AA)$_n$

With the aim of synthesizing and evaluating biocompatible and dual stimulus-responsive block copolymers, we selected p(MPC) and poly(L-aspartic acid) (p(AA)) as the building blocks. Importantly, p(MPC) is among the most biocompatible polymers known. To date, several p(MPC)-based therapeutics including therapeutic proteins [46], anti-cancer drug conjugates [47], and block copolymer micelles [48, 49] or vesicles [50,51] have been studied. p(AA) is a biodegradable polypeptide containing free carboxylic acid groups in the chain. These carboxylic acid groups are protonated at pH below 5.0 but are ionized at pH above 5.0 as the pKa of p(AA) is 4.88 [51]. Its biodegradability and pH-sensitive properties [52] make p(AA) an ideal molecule to combine with p(MPC) in the design of an effective and sensitive drug delivery system. To the best of our knowledge, this is the first report of redox and pH dual-responsive p(MPC)−*b*−p(AA) block copolymers developed for the intracellular delivery of Dox.

RAFT has already been successfully employed with copper-catalyzed azide-alkyne cycloaddition in polymer synthesis by introducing azides and alkyne groups either as end groups or as monomers [53−55]. Herein, for the synthesis of p(MPC)$_{50}$−*b*−p(AA)$_n$, azide-terminated p(MPC)$_{50}$ was subjected to click cycloaddition reactions under "strict click conditions" with alkyne terminated p(BLA)$_n$, to yield p(MPC)–*b*–p(BLA)$_n$ (n = 10, 25, 50, 75). The protective

side-chains of the polymers were removed by treating with HBr/AcOH in trifluoroacetic acid and subsequent aminolysis to remove the thiocarbonylthio end groups. After precipitation in diethyl ether, $p(MPC)_{50}$−*b*−$p(AA)_n$ was further purified by dialysis against DI water and the pure product isolated after lyophilization. The block copolypeptides were characterized by ^{1}H NMR spectroscopy (see Fig. S6 of SM). The composition and the MW of the block copolypeptides are provided in Table 1.

3.4. Fabrication of and characterization of $p(MPC)_{50}$−b−$p(AA)_n$ vesicles

Herein, we demonstrated the fabrication of vesicles by the self-assembly of $p(MPC)_{50}$−*b*−$p(AA)_n$ hybrid block copolymers. In order to investigate the self-assembling behavior, we selected block copolymers with a large number of aspartic acid units (n = 50, 75). After careful examination of polymer solubility, an ethanol-water solvent combination was selected for the fabrication of the vesicles. It was identified that, the copolymers with a less aspartic acid units displayed enhanced solubility in water, and thus prevented the formation of stable vesicle structures through self-assembly in aqueous media. Self-assembly occurred after injection of aqueous buffer into the ethanolic polymer solution, a step that exploited the solubility difference of p(MPC) and p(AA) blocks in water and ethanol. After removal of ethanol by dialysis, the morphologies of the self-assembled vesicles were characterized. We found that the amount of aqueous buffer injected determined the nature of the formation of the vesicles. It was determined that addition of 300 µL of aqueous buffer to 700 µL of polymer in ethanol (1 mg/mL concentration) was the most ideal for the formation of uniform vesicles. Dialysis against deionized water was conducted to remove unloaded Dox and ethanol, and the Dox loading content and loading efficiency of the vesicles were determined (Table 2). Dox encapsulated in

the vesicles of $p(MPC)_{50}$−*b*−$p(AA)_{75}$ were utilized for the, *in vitro* release, and cellular internalization studies.

The pH and redox-responsive size change of the $p(MPC)_{50}$−*b*−$p(AA)_{75}$ vesicles was confirmed by a set of DLS experiments. At physiological conditions (pH 7.4 and 37 °C) a uniform particle size of 100 nm was observed (Fig. 1(a)). Measurement 4 h later, after adjusting the pH of the vesicle dispersion to that of the endosomal range (pH 5.5), revealed that the particle size had significantly increased (Fig. 1(b)) i.e., there was a pH-induced swelling of the vesicles. Interestingly, in this endosomal pH range, addition of 10 mM DTT caused a further increase in size when measured after 4 h (~800 nm) and a broad distribution was observed (Fig. 1(c)). This phenomenon was attributed to the synergistic effect of the reductive cleavage of the SS bond together with the pH-induced swelling of the vesicles. Finally, the morphology of the $p(MPC)_{50}$−*b*−$p(AA)_n$ (n= 50, 75) vesicles fabricated at pH 7.4 were visualized by TEM. As shown in Fig. 2, spherical vesicles of around 100 nm were clearly observed and this was consistent with the size analysis by DLS.

3.5. Stimuli-responsive Release of Dox from $p(MPC)_{50}$−b−p(AA) Vesicles

Dox is widely used to treat a broad range of solid malignant tumors. Herein, Dox was used as a model drug to evaluate the in vitro drug release behavior from loaded $p(MPC)_{50}$−*b*−$p(AA)_{75}$ vesicles. Dox was loaded into the vesicles through a dialysis method; the DLC and DLE were determined to be 19.8% and 66%, respectively (Table 2). The time-dependent release performance of Dox under different pH conditions and different DTT concentrations was investigated in $p(MPC)_{50}$−*b*−$p(AA)_{75}$ vesicles in PBS. Dox release was evaluated by UV-Vis spectrometry at 480 nm which is the characteristic absorption maximum of Dox in solution. The release performance was assessed over 72 h; release profiles are shown in Fig. 3. At pH 7.4, Dox

loaded $p(MPC)_{50}$−*b*−$p(AA)_{75}$ vesicles at different DTT concentrations (5, 10, 15 mmol) displayed a suppressed Dox release profile compared to the corresponding experiment conducted at pH 5.5. As shown in Fig. 3(a), it is obvious that only about 15%, 31% and 44% of Dox was released in 72 h, at 5, 10, and 15 mmol DTT, respectively.

On the other hand, at pH 5.5, the Dox release rate was much faster and within 72 h, 61% ,70%, and 76% of the initial Dox load was released at 5, 10, 15 mmol DTT, respectively (Figure 3(b)). Importantly, at pH 5.5, Dox release is found to be more effective at all DTT concentrations when compared with that at pH 7.4 at the corresponding DTT concentrations. The highest Dox release rate was observed when dual stimuli (pH 5.5 and addition of 15 mmol of DTT) were applied. The dual-stimuli responsive Dox release phenomenon is related to the structural disassembly of the $p(MPC)_{50}$−*b*−$p(AA)_{75}$ vesicles. While a lower pH led to swelling of the Dox-loaded vesicles due to the protonation of the carboxyl groups in p(AA) segments, the concurrent addition of DTT resulted in vesicle disassembly caused by the cleavage of the SS linker. These release profiles clearly indicated a desirable pH and reduction sensitivity for intracellular delivery. In other words, the vesicle could hold a substantial amount of encapsulated Dox over an extended period during systemic circulation (pH 7.4) but rapid release of the drug can be triggered by the tumoral acidic and reductive environment.

3.6. Cytotoxicity of $p(MPC)_{50}$–b–$p(AA)_n$ vesicles

Investigation of the effect of blank vesicles on cell viability is important prior to the *in vitro* and *in vivo* Dox internalization studies. The effect of $p(MPC)_{50}$–*b*–$p(AA)_n$ vesicles on the viability of NIH 3T3 and 4T1 cell lines was determined using an MTS cell viability assay. The cell-only group was used as the positive control (P.C.) and Triton X100-treated cells were used as the negative control (N.C.). The effect of $p(MPC)_{50}$–*b*–$p(AA)_n$ vesicles on the viability of NIH

3T3 and 4T1 cell lines was assessed over a wide range (1−100 μg/mL) of polymer concentrations. Results revealed no significant effect on cell viability profiles upon treatment with p(MPC)$_{50}$–*b*–p(AA)$_n$ polymers regardless of the chain length of p(AA). Polymer-treated NIH 3T3 and 4T1 cells showed high viability (>95%) even at the highest exposure levels (Fig. 4). From the results of the in vitro studies, it was evident that p(MPC)$_{50}$–*b*–p(AA)$_n$ polymers had no acute and intrinsic cytotoxicity against normal (NIH 3T3) or cancer cell lines (4T1) irrespective of their structural composition

3.7. Cellular uptake and intracellular release of Dox

To examine the anticancer effect of the Dox-encapsulated p(MPC)–*b*–p(AA) vesicles against cancer cells, Dox-encapsulated p(MPC)$_{50}$-*b*-p(AA)$_{75}$ vesicles were administered to 4T1 cancer cells over 24 h. The Dox-loaded vesicles underwent disassembly, due to the synergistic effects of redox- and pH stimulus-responsiveness, and displayed a dose-dependent (0.2−100 μg/mL of Dox concentration) cytotoxicity against the 4T1 cell lines. The enhanced toxicity and cell death that was observed in the endosomal pH range (pH 5.5) highlighted the increased intracellular release of Dox from the vesicles at that pH when compared with that occurring at pH 7.4. Note that, at pH 5.5, the clear stimulus-responsive release of Dox resulted in a dose-dependent anticancer effect from 6.2 μg/mL Dox upwards (Fig. 5(A)).

Confocal microscopic experiments were performed to visualize the intracellular uptake and redox- and pH-responsive intracellular release of Dox from the vesicles into 4T1 cancer cells. As shown in Fig. 5(B), at pH 5.5 (g–i) a stronger fluorescence of Dox was observed when compared with that observed at pH 7.4 (d–f) compared to the control experiments (a–c). Similar experiments with free Dox showed low intracellular internalization due to the lack of stimuli responsiveness (Fig. S7(A)). To obtain confirmation of the observed intracellular internalization,

cells treated with Dox- loaded p(MPC)$_{50}$–*b*–p(AA)$_{75}$ vesicles and with free Dox were subjected to quantitative analysis using flow cytometry (FACScan).

The FACScan analysis results of the Dox-loaded p(MPC)$_{50}$–*b*–p(AA)$_{75}$ treated 4T1 cells are provided in Fig. 5(C). It is also evident that the enhanced fluorescence intensity is observed at the endosomal pH rather than at the physiological pH. From these results, we concluded that the vesicles are able to efficiently release Dox via reduction and pH dual stimuli-induced disassembly, and that they can specifically release Dox into tumor cells. On the other hand, the FACScan analysis of cells treated only with free Dox showed poor intracellular uptake (Fig. S7(B)).

4. Conclusions

In this study, we successfully synthesized a series of pH and reduction dual stimuli-responsive block copolymers p(MPC)$_{50}$–*b*–p(AA)$_n$ by utilizing RAFT, ring opening polymerization of amino acid NCAs, and azide−alkyne click cycloaddition reactions. Vesicles self-assembled from the copolymer have pH and reduction responsiveness as verified by DLS. The p(MPC)–*b*–p(AA) copolymer vesicles were effectively internalized into NIH 3T3 and 4T1 cell lines. The viability of both cell lines was >95% at an extensive range of polymer concentrations (1−100 μg/mL). The Dox-encapsulated vesicles preferentially released Dox in 4T1 tumor cells as confirmed by CLSM and FACScan analysis. The prepared vesicles are nontoxic, and showed a good loading efficiency of Dox. They could rapidly cross cell membranes and release Dox into cancer cells by endosomal pH reduction-induced disassembly. These vesicles fabricated were showing pH and reduction dual-responsiveness, hold great promise as intracellular anticancer drug delivery systems.

Acknowledgements

This work was supported by the Basic Science Research Program through the National Research Foundation of Korea (2015R1D1A1A09057372). The authors also thank to the Bio & Medical Technology Development Program of the NRF funded by the Korean government, MSIP (2016M3A9E8942069).

Appendix A. Supplementary material

Supplementary data associated with this article can be found in a separated file.

References

[1] N. Larson, H. Ghandehari, Polymeric conjugates for drug delivery, Chem. Mater. 24 (2012) 840–853.

[2] S. Cai, Q. Yang, T.R. Bagby, M. L. Forrest, Lymphatic drug delivery using engineered liposomes and solid lipid nanoparticles, Adv. Drug Delivery Rev. 63 (2011) 901–908.

[3] K. Kataoka, A. Harada, Y Nagasaki, Block copolymer micelles for drug delivery: Design, characterization and biological significance, Adv. Drug Delivery Rev. 64 (2012) 37–48.

[4] R. P. Johnson, Y-I. Jeong, E. Choi, C-W. Chung, D. H. Kang, S-O. Oh, H. Suh, I. Kim, Biocompatible poly(2-hydroxyethyl methacrylate)-b-poly(L-histidine) hybrid materials for pH-sensitive intracellular anticancer drug delivery, Adv. Funct. Mater. 22 (2012) 1058–1068.

[5] R. P. Johnson, Y-I. Jeong, J. V. John, C-W. Chung, D. H. Kang, M. Selvaraj, H. Suh, I. Kim, Dual stimuli-responsive poly(N-isopropylacrylamide)-b-poly(l-histidine) chimeric materials for the controlled delivery of doxorubicin into liver carcinoma, Biomacromolecules 14 (2013) 1434–1443.

[6] F. H. Meng, Z. Y. Zhong, J. Feijen, Stimuli-responsive polymersomes for programmed drug delivery, Biomacromolecules 10 (2009) 197–209.

[7] L. Zhao, N. Li, K. Wang, C. Shi, L. Zhang, Y. Luan, A review of polypeptide-based polymersomes, Biomaterials 35 (2014) 1284–1301.

[8] M. A. Phillips, M. L. Gran, N. A. Peppas, Targeted nanodelivery of drugs and diagnostics, Nano Today 5 (2010) 143–159.

[9] J. Fang, H. Nakamura, H. Maeda, The EPR effect: Unique features of tumor blood vessels for drug delivery, factors involved, and limitations and augmentation of the effect, Adv. Drug Delivery Rev. 63 (2011) 136–151.

[10] T. L.; Andresen, S. S.; Jensen, K. Jorgensen, Advanced strategies in liposomal cancer therapy: problems and prospects of active and tumor specific drug release, Prog. Lipid Res. 44 (2005) 68–97.

[11] A. Gabizon, A. Shmeeda, S. Zalipsky, Pros and cons of the liposome platform in cancer drug targeting, J. Liposome Res. 16 (2006) 175–183.

[12] A. L. B. Seynhaeve, S. Hoving, D. Schipper, C. E. Vermeulen, G. A. de Wiel-Ambagtsheer, S. T. van Tiel, A. M. M. Eggermont, T. L. M. ten Hagen, Tumor necrosis factor alpha mediates homogeneous distribution of liposomes in murine melanoma that contributes to a better tumor response, Cancer Res. 2007, 67, 9455–9462.

[13] W. N. Joseph, Y. H. Bae, Odyssey of a cancer nanoparticle: From injection site to site of action, Nano Today 7 (2012) 606–618.

[14] R. P. Johnson, J. V. John, I. Kim, Poly(l-histidine)-containing polymer bioconjugate hybrid materials as stimuli-responsive theranostic systems, J. Appl. Polym. Sci. 131 (2014) 40796.

[15] T. Kaiden, E. Yuba, A. Harada, Y. Sakanishi, K. Kono, Dual signal-responsive liposomes for temperature-controlled cytoplasmic delivery, Bioconjugate Chem. 22 (2011) 1909–1915.

[16] C. S. Lee, W. Park, S. Park, K. Na, Endolysosomal environment-responsive photodynamic nanocarrier to enhance cytosolic drug delivery via photosensitizer-mediated membrane disruption, Biomaterials 34 (2013) 9227–9236.

[17] R. Cheng, F. Feng, F. Meng, C. Deng, J. Feijen, Z. Zhong, Glutathione-responsive nano-vehicles as a promising platform for targeted intracellular drug and gene delivery, J. Control. Release 152 (2011) 2–12.

[18] P. Watson, A. T. Jones, D. J. Stephens, Intracellular trafficking pathways and drug delivery: fluorescence imaging of living and fixed cells, Adv. Drug Delivery Rev. 57 (2005) 43–61.

[19] M. Hrub, C. Konak, K. Ulbrich, Polymeric micellar pH-sensitive drug delivery system for doxorubicin, J. Control. Release 103 (2005) 137–148.

[20] M. S. Kim, S. J. Hwang, J. K. Han, E. K. Choi, H. J. Park, J. S. Kim, D. S. Lee, pH-responsive PEG-poly(β-amino ester) block copolymer micelles with a sharp transition, Macromol. Rapid Commun. 27 (2006) 447–451.

[21] S. Dai, P. Ravi, K. C. Tam, pH-Responsive polymers: synthesis, properties and applications, Soft Matter 4 (2008) 435–449.

[22] R. P. Johnson, C-W. Chung, Y-I. Jeong, D. H. Kang, H. Suh, I. Kim, Poly(L-histidine)-tagged 5-aminolevulinic acid prodrugs: new photosensitizing precursors of protoporphyrin IX for photodynamic colon cancer therapy, Int. J. Nanomed. 7 (2012) 2497–2512.

[23] R. P. Johnson, Y-I. Jeong, J. V. John, C-W Chung, S. H. Choi, S. Y. Song, D. H. Kang, H. Suh, I. Kim, Lipo-poly(L-histidine) hybrid materials with pH-sensitivity, intracellular delivery

efficiency, and intrinsic targetability to cancer cells, Macromol. Rapid Commun. 35 (2014) 888–894.

[24] F. H. Meng, W. E. Hennink, Z. Zhong, Reduction-sensitive polymers and bioconjugates for biomedical applications, Biomaterials 30 (2009) 2180–2198.

[25] F. Q. Schafer, G. R. Buettner, Redox environment of the cell as viewed through the redox state of the glutathione disulfide/glutathione couple, Free Radic. Biol. Med. 30 (2001) 1191–1212.

[26] H. F. Gilbert, Thiol/disulfide exchange equilibria and disulfide bond stability, Methods Enzymol. 1995, 251, 8–28.

[27] P. Kuppusamy, M. Afeworki, R. A. Shankar, D. Coffin, M. C. Krishna, S. M. Hahn, J .B. Mitchell, J. L. Zweier, *In vivo* electron paramagnetic resonance imaging of tumor heterogeneity and oxygenation in a murine model, Cancer Res. 58 (1998) 1562–1568.

[28] B. M. Discher, Y. Y. Won, D. S. Ege, J. C. M. Lee, F. S. Bates, D. E. Discher, D. A. Hammer, Polymersomes: tough vesicles made from diblock copolymers, Science 284 (1999) 1143–1146.

[29] C. LoPresti, H. Lomas, M. Massignani, T. Smart, G. Battaglia, Polymersomes: nature inspired nanometer sized compartments, J. Mater. Chem. 19 (2009) 3576–3590.

[30] H. Kukula, H. Schlaad, M. Antonietti, S. Forster, The formation of polymer vesicles or "peptosomes" by polybutadiene-block-poly(l-glutamate)s in dilute aqueous solution, J. Am. Chem. Soc. 124 (2002) 1658–1663.

[31] F. Checot, A. Brulet, J. Oberdisse, Y. Gnanou, O. Mondain-Monval, S. Lecommandoux, Structure of polypeptide-based diblock copolymers in solution: stimuli-responsive vesicles and micelles, Langmuir 21 (2005) 4308–4315.

[32] R. Sigel, M. Losik, H. Schlaad, pH responsiveness of block copolymer vesicles with a polypeptide corona, Langmuir 23 (2007) 7196–7199.

[33] J. Rodrıguez-Hernandez, S. Lecommandoux, Reversible Inside−Out Micellization of pH-responsive and water-soluble vesicles based on polypeptide diblock copolymers, J. Am. Chem. Soc. 127 (2005) 2026–2027.

[34] K. K. Upadhyay, J-F. Le Meins, A. Misra, P. Voisin, V. Bouchaud, E. Ibarboure, C. Schatz, S. Lecommandoux, Biomimetic doxorubicin loaded polymersomes from hyaluronan-block-poly(γ-benzyl glutamate) copolymers, Biomacromolecules 10 (2009) 2802–2808.

[35] K. K. Upadhyay, A. N. Bhatt, A. K. Mishra, B. S. Dwarakanath, C. Schatz, J−F. Le Meins, A. Farooque, G. Chandraiah, A. K Jain, A. Misra, S. Lecommandoux, The intracellular drug delivery and anti-tumor activity of doxorubicin loaded poly(γ-benzyl l-glutamate)-b-hyaluronan polymersomes, Biomaterials 31 (2010) 2882–2892.

[36] C. Sanson, C. Schatz, J-F. Le Meins, A. Soum, J. Thevenot, E. Garanger, S. Lecommandoux, A simple method to achieve high doxorubicin loading in biodegradable polymersomes, J. Control. Release 147 (2010) 428–435.

[37] C. Sanson, O. Diou, J. Thevenot, E. Ibarboure, A. Soum, A. Brulet, S. Miraux, E. Thiaudière, S. Tan, A. Brisson, V. Dupuis, O. Sandre, S. Lecommandoux, Doxorubicin loaded magnetic polymersomes: theranostic nanocarriers for MR imaging and magneto-chemotherapy, ACS Nano 5 (2011) 1122−1140.

[38] R. P. Johnson, S. Uthaman, J. V. John, H. R. Lee, S. J. Lee, H. Park, I-K. Park, H. Suh, I. Kim, Poly(PEGA)-b-poly(l-lysine)-b-poly(l-histidine) hybrid vesicles for tumoral pH-triggered intracellular delivery of doxorubicin hydrochloride, ACS Appl. Mater. Interfaces 7 (2015) 21770−21779.

[39] G. Bayramoglu, D. Gozen, G. Ersoy, V. C. Ozalp, K. C. Akcali, M. Y. Arica, Examination of fabrication conditions of acrylate-based hydrogel formulations for doxorubicin release and efficacy test for hepatocellular carcinoma cell, J. Biomater Sci. Polym Ed. 25 (2014) 657−78.

[40] S. Y. Kim, I. G. Shin, Y. M. Lee, Amphiphilic diblock copolymeric nanospheres composed of methoxy poly(ethylene glycol) and glycolide: properties, cytotoxicity and drug release behavior, Biomaterials 20 (1999) 1033–1042.

[41]. G. Bayramoglu, M. Yılmaz, E. Batislam, M. Y. Arıca, Heparin-coated poly(hydroxyethyl methacrylate/albumin) hydrogel networks: In vitro hemocompatibility evaluation for vascular biomaterials, J. Appl. Polym. Sci. 109 (2008) 749−757.

[42] S. Chen, J. Zheng, L. Li, S. Jiang, Strong resistance of phosphorylcholine self-assembled monolayers to protein adsorption: Insights into nonfouling properties of zwitterionic materials. J. Am. Chem. Soc. 127 (2005) 14473−14478.

[43] G. Hu, T. Emrick, Functional choline phosphate polymers, J. Am. Chem. Soc. 138 (2016) 1828−1831.

[44] V. Ladmiral, T. M. Legge, Y. Zhao, S. Perrier “Click” chemistry and radical polymerization: potential loss of orthogonality, Macromolecules 41 (2008) 6728−6732.

[45] X. Jiang, N. J. Liu, L. Xu, R. Zhuo, Disulfide-containing hyperbranched polyethylenimine derivatives via click chemistry for nonviral gene delivery, Macromol. Chem. Phys. 212 (2011) 64−71.

[46] A. Lewis, Y. Tang, S. Brocchini, J-W. Choi, A. Godwin, Poly(2-methacryloyloxyethyl phosphorylcholine) for protein conjugation, Bioconjugate Chem. 19 (2008) 2144−2155.

[47] S. M. Page, E. Henchey, X. Chen, S. Schneider, T. Emrick, Efficacy of PolyMPC–DOX prodrugs in 4T1 tumor-bearing mice, Mol. Pharmaceutics 11 (2014) 1715−1720.

[48] S. M. Page, M. Martorella, S. Parelkar, I. Kosif, T. Emrick, Disulfide cross-linked phosphorylcholine micelles for triggered release of camptothecin, Mol. Pharmaceutics 10 (2013) 2684−2692.

[49] J. Du, Y. Tang, A. L. Lewis, S. P. Armes, pH-Sensitive vesicles based on a biocompatible zwitterionic diblock copolymer, J. Am. Chem. Soc. 127 (2005) 17982− 17983.

[50] H. Lomas, J. Du, I. Canton, J. Madsen, N. Warren, S. P. Armes, A. L. Lewis, G. Battaglia, Efficient encapsulation of plasmid DNA in pH-sensitive PMPC-PDPA polymersomes: study of the effect of PDPA block length on copolymer-DNA binding affinity, Macromol. Biosci. 10 (2010) 513−530.

[51] C. Wang, L. Wang, W. Yang, Preparation and characterization of functional inorganic/organic composite microspheres via electrostatic interaction, J. Colloid Interface Sci. 333 (2009) 749−756.

[52] C. H. Liu, Y. Q. Chen, J. G. Chen, Preparation and characterization of pH-sensitive hydrogel for drug delivery system, Carbohydr. Polym. 79 (2010) 500−506.

[53] D. Quemener, T. P. Davis, C. Barner-Kowollik, M. H Stenzel, Rapid synthesis of block and cyclic copolymers via click chemistry in the presence of copper nanoparticles, Chem. Commun. 48 (2006) 5051−5053.

[54] J. Zhu, X. Zhu, E. T. Kang, K.G. Neoh, Design and synthesis of star polymers with hetero-arms by the combination of controlled radical polymerizations and click chemistry, Polymer 48 (2007) 6992−6999.

[55] Y. Li, J. Yang, B. C. Benicewicz, Well-controlled polymerization of 2-azidoethyl methacrylate at near room temperature and click functionalization, J. Polym. Sci., Part A: Polym. Chem. 45 (2007) 4300−4308.

Tables

Table 1. Molecular characteristic of $p(MPC)_{50}$–*b*–$p(AA)_n$ block copolymers synthesized by azide-alkyne click cycloaddition reaction.

Block copolymer	$M_n \times 10^{-4}$(g/mol)		Yield (%)
	Theoretical	NMR	
$p(MPC)_{50}$–*b*–$p(AA)_{10}$	1.55	1.42	58
$p(MPC)_{50}$–*b*–$p(AA)_{25}$	1.91	1.78	66
$p(MPC)_{50}$–*b*–$p(AA)_{50}$	2.42	2.31	62
$p(MPC)_{50}$–*b*–$p(AA)_{75}$	2.95	2.83	60

Table 2. The behaviors of blank and Dox loaded vesicles of $p(MPC)_{50}$-*b*-$p(AA)_{75}$ at different pHs.

Block copolymer	pH	Blank vesicles		Dox-loaded vesicles at 20:1 (w/w)[a]		DLC (%)	DLE (%)
		D_H (nm)	$Đ$	D_H (nm)	$Đ$		
$p(MPC)_{50}$–*b*–	7.4	110±1.6	0.24	240±2.1	0.23	19.8	66.0

$p(AA)_{75}$	5.5	280±1.8	0.46	320±1.3	0.38

[a] Feed ratio of polymer to Dox. Dox loading experiments were performed using PBS (pH 10.5).

Scheme and Figure Captions

Scheme 1. Synthetic route of $p(MPC)_{50}$–*b*–$p(AA)_n$ block copolypeptides by the click cycloaddition reaction of azide-terminated p(MPC) and alkyne-terminated p(BLA).

Fig. 1. Size variation, based on DLS measurements, of $p(MPC)_{50}$–*b*–$p(AA)_{75}$ vesicles in response to pH and addition of DTT (a) at pH 7.4 and (b) at pH 5.5 after 4 h, and (c) at pH 5.5 and 10 mM DTT after 4 h.

Fig. 2. TEM images of $p(MPC)_{50}$–*b*–$p(AA)_{75}$ vesicles obtained by self-assembly in ethanol/water solvent mixture: (a) at pH 7.4, (b) at pH 5.5, and (c) at pH 5.5 in the presence of 5 mmoL DTT.

Fig. 3. The time-dependent release of Dox from $p(MPC)_{50}$–*b*–$p(AA)_{75}$ vesicles in phosphate-buffered saline (PBS) at 37 ^{o}C and at different DTT concentrations (a) pH 7.4 and (b) pH 5.5.

Fig. 4. Cell viability measured by the MTS assay of (a) NIH 3T3 and (b) 4T1 cells treated with $p(MPC)_{50}$–*b*–$p(AA)_n$ at different concentrations. The cell-only group was used as the positive control (P.C), and Triton X100 was used as negative control (N.C).

Fig. 5. (A) Dose-dependent antitumor activity of Dox-loaded $p(MPC)_{50}$–*b*–$p(AA)_{75}$ vesicles against 4T1 cells after 24 h incubation at pH 7.4 and 5.5. (B) Confocal laser scanning microscopic images of 4T1 cells taken after 4 h incubation at pH 7.4 (d–f) and pH 5.5 (g–i) with

Dox-loaded p(MPC)$_{50}$–*b*–p(AA)$_{75}$ vesicles (Dox = 15 μg/mL). (C) Flow cytometric analysis of 4T1 cells after treatment with p(MPC)$_{50}$–*b*–p(AA)$_{75}$ vesicles.

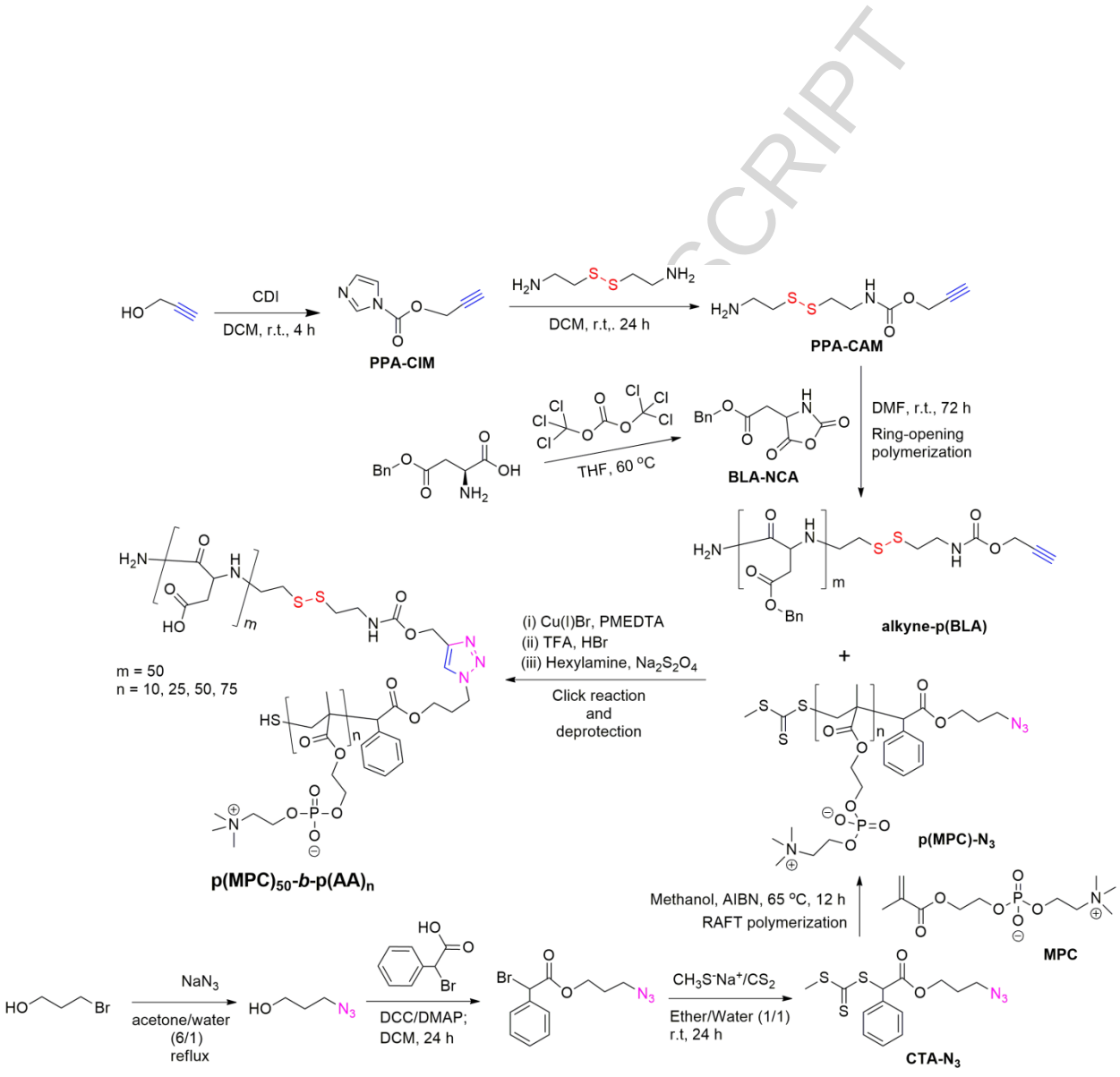

Scheme 1. Synthetic route of p(MPC)$_{50}$–*b*–p(AA)$_n$ block copolypeptides by the click cycloaddition reaction of azide-terminated p(MPC) and alkyne-terminated p(BLA).

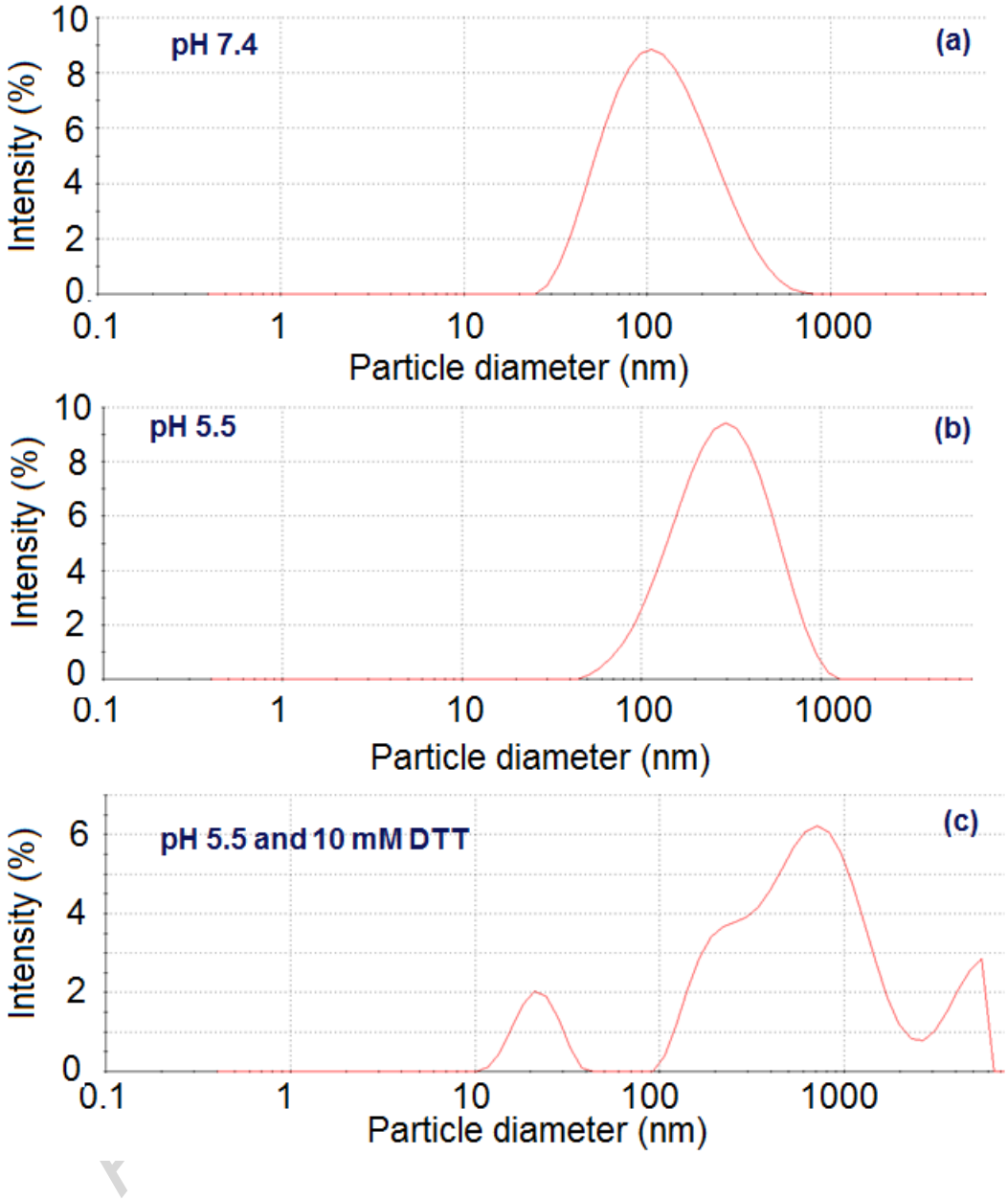

Fig. 1. Size variation, based on DLS measurements, of $p(MPC)_{50}$–*b*–$p(AA)_{75}$ vesicles in response to pH and addition of DTT (a) at pH 7.4 and (b) at pH 5.5 after 4 h, and (c) at pH 5.5 and 10 mM DTT after 4 h.

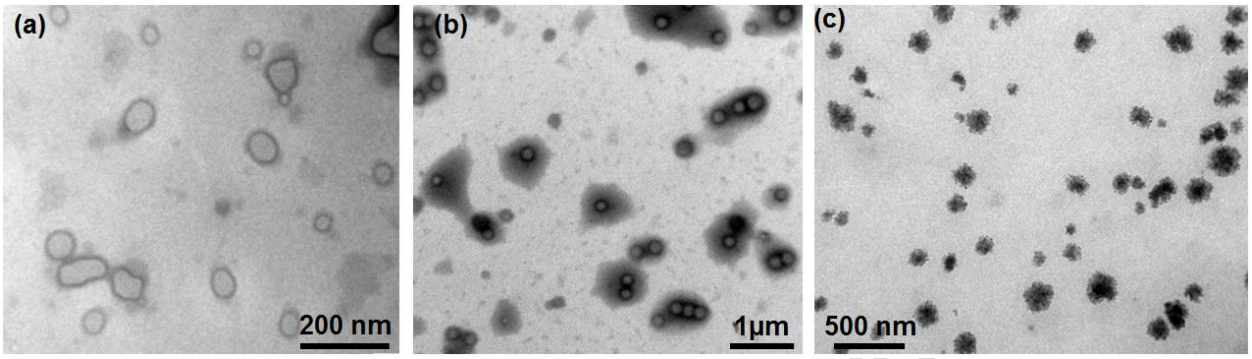

Fig. 2. TEM images of $p(MPC)_{50}$–*b*–$p(AA)_{75}$ vesicles obtained by self-assembly in ethanol/water solvent mixture: (a) at pH 7.4, (b) at pH 5.5, and (c) at pH 5.5 in the presence of 5 mmoL DTT.

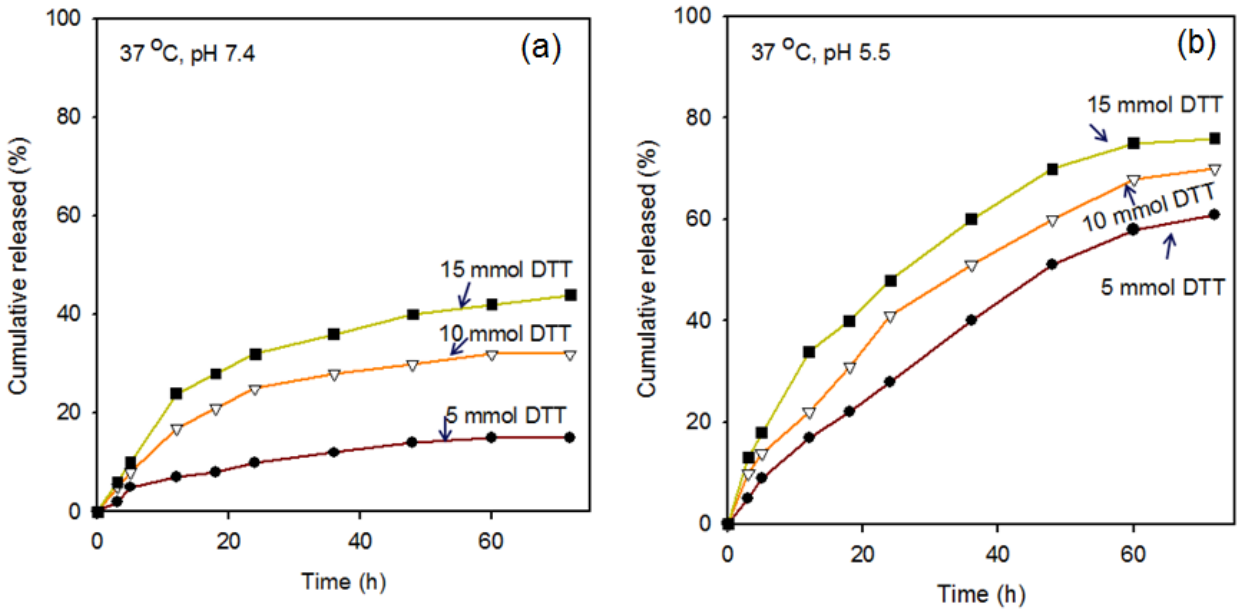

Fig. 3. The time-dependent release of Dox from $p(MPC)_{50}$–*b*–$p(AA)_{75}$ vesicles in phosphate-buffered saline (PBS) at 37 °C and at different DTT concentrations (a) pH 7.4 and (b) pH 5.5.

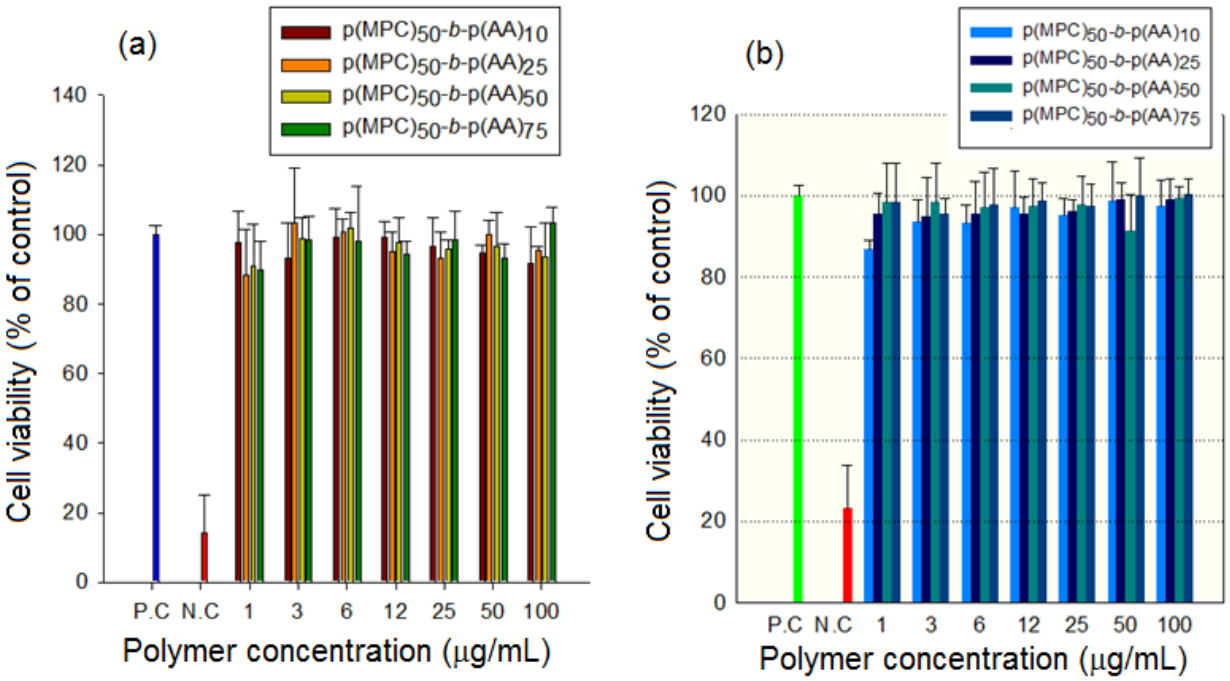

Fig. 4. Cell viability measured by the MTS assay of (a) NIH 3T3 and (b) 4T1 cells treated with $p(MPC)_{50}$–*b*–$p(AA)_n$ at different concentrations. The cell-only group was used as the positive control (P.C), and Triton X100 was used as negative control (N.C).

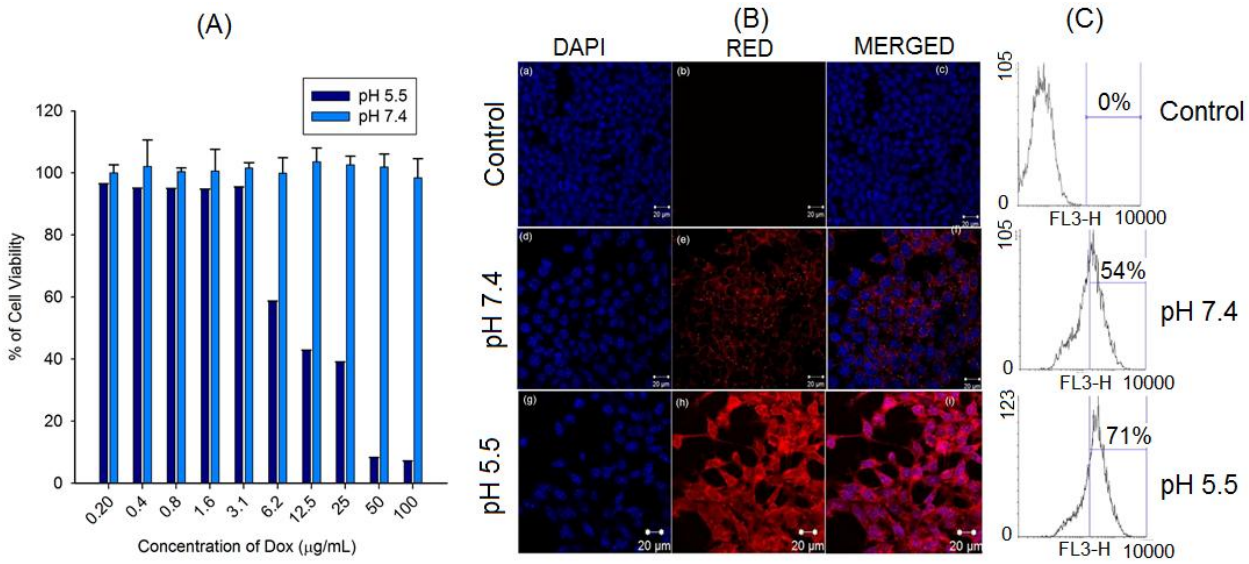

Fig. 5. (A) Dose-dependent antitumor activity of Dox-loaded p(MPC)$_{50}$–*b*–p(AA)$_{75}$ vesicles against 4T1 cells after 24 h incubation at pH 7.4 and 5.5. (B) Confocal laser scanning microscopic images of 4T1 cells taken after 4 h incubation at pH 7.4 (d–f) and pH 5.5 (g–i) with Dox-loaded p(MPC)$_{50}$–*b*–p(AA)$_{75}$ vesicles (Dox = 15 μg/mL). (C) Flow cytometric analysis of 4T1 cells after treatment with p(MPC)$_{50}$–*b*–p(AA)$_{75}$ vesicles.

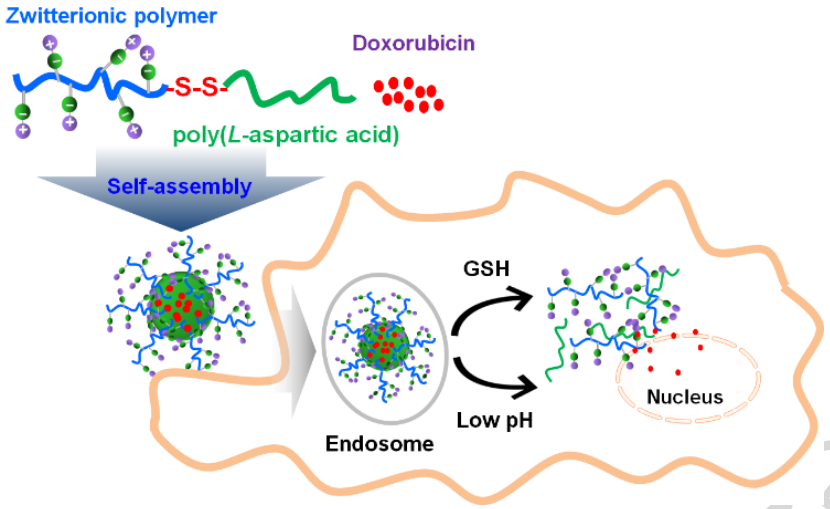

Graphical abstract

Highlights

- Zwitterionic polymer block poly(*L*-aspartic acid) hybrids were synthesized
- Redox/pH dual-responsive drug delivery was evaluated
- The dual-responsive nanovesicles displayed dose-dependent cytotoxicity in 4T1 cancer cells